Steel and Composite Structures, *Vol. 26, No. 4* (*2018*) *501-511*
DOI: https://doi.org/10.12989/scs.2018.26.4.501

Behavior of circular concrete-filled steel tubular columns under pure torsion

Fa-xing Ding [1], Qiang Fu [1], Bing Wen [1], Qi-shi Zhou [*1] and Xue-mei Liu [2]

[1] *School of Civil Engineering, Central South University, Changsha 410075, P.R. China*
[2] *School of Civil Engineering and Built Environment, Queensland University of Technology, Brisbane, QLD 4001, Australia*

(*Received June 21, 2016, Revised November 9, 2017, Accepted December 15, 2017*)

Abstract. Concrete-filled steel tubular (CFT) columns are commonly used in engineering structures and always subjected to torsion in practice. This paper is thus devoted to investigate the mechanical behavior of circular CFT columns under pure torsion.3D finite element models based on reasonable material constitutive relation were established for analyzing the load-strain (T–γ) curves of circular CFT columns under pure torsion. The numerical simulation indicated that local bulking of the steel tube in CFT columns was prevented and the shear strength and ductility of the core concrete were significantly improved due to the confinement effect between the steel tube and the core concrete. Based on the results, formulas to predict the torsional ultimate bearing capacity of circular CFT columns were proposed with satisfactory correspondence with experimental results. Besides, formulas of composite shear stiffness and the overall process of the T–γ relation of circular CFT columns under pure torsion were proposed.

Keywords: concrete-filled steel tube (CFT); pure torsion; finite element; ultimate bearing capacity; confinement effect

1. Introduction

Concrete-filled steel tubular (CFT) column is a composite member formed by a steel tube filled with concrete, which ideally combines the advantages of both steel and concrete and provides excellent structural properties such as high strength, high ductility, large energy absorption capacity and easy construction (Lee *et al*. 2011, Chang *et al*. 2013, Wang and Chang 2013, Kim *et al*. 2016 and Kwak *et al.* 2013, Kim *et al*. 2017). But in practice, the piers of curved bridges, skew bridges and some other complex engineering structures, where circular CFT columns are widely used, are always subjected to torsion. Therefore, the mechanical behavior of circular CFT columns under pure torsion needs to be considered and analyzed.

Few studies on circular CFT columns under pure torsion have been found in literature in the past few years. Xu and Zhou (1991) experimented three circular concrete-filled steel tubular columns with different steel ratio under pure torsion and proposed formula to compute the ultimate bearing capacity of specimens based on superposition method. Han ~~and Yao~~ *et al.* (2007) conducted experimental and theoretical studies on the nonlinear torsional behavior of circular and square CFT columns, and a comparison of results calculated using finite element method showed good agreement with test results. The bearing capacity standard of CFT columns under pure torsion were defined and simplified design method were proposed by regression method to calculate the ultimate bearing capacity. Besides, the simplified composite shear modulus formulas were proposed too. Beck and Kiyomiya (2003) carried out experimental research on three CFT members with circular section under pure torsion and found that the ultimate bearing capacity was greatly enhanced as the core concrete added stiffness to the steel tube and the local bulking was prevented. Lee *et al.* (2009) investigated the behavior of circular CFT column under combined torsion and compression considering the confinement effect of the steel tube, softening of concrete, and spiral effects. Biaxial stress effects due to diagonal cracking were also considered. At last, a basic equation to describe the torsional behavior of the entire loading history of CFT members was derived. Nie *et al.* (2012) based on the quasi-static test on CFT columns subjected to pure torsion and compression–torsion cyclic load, the torsion behavior of CFT columns with various section types, steel ratio and axial load were studied. When CFT columns subjected to pure torsion, spiral diagonal compressive struts was created in the in-filled concrete, and the axial components of the diagonal compressive force of the in-filled concrete was equal to the axial tensile force of the steel tube to satisfy the axial load equilibrium condition. Based on the test results, the torsion mechanism of CFT columns were preliminarily analyzed. Kwak *et al.* (2008) studied the behavior and design of thin-walled centrifugal CFT columns under pure torsion. The test results showed that design strengths predicted by standards were conservative.

However, available studies on CFT columns under pure torsion are limited and necessitate further investigation for certain issues, one of which is the confinement effect between the steel tube and the core concrete on the torsional behavior of CFT columns. Besides, the available formulas to predict the ultimate bearing capacity of circular CFT columns under pure torsion varied in forms and precisions

*Corresponding author, Professor,
E-mail: qishizhou@csu.edu.cn

ISSN: 1229-9367 (Print), 1598-6233 (Online)

and need comparison and optimization. In addition, the formula of composite shear stiffness of CFT columns is merely addressed in design code in a modified form and the influence of plastic development of the core concrete under pure torsion was not analyzed in existing literature.

Therefore, to solve the above-mentioned problems, this paper is devoted to investigate the mechanical behavior of circular CFT columns under pure torsion. The main objectives of this paper are as follows: (1) To establish full-scale models to carry out extensive parametric studies on the mechanical performance of circular CFT columns under pure torsion on the basis of the validated finite element models; (2) To analyze the confinement effect between the steel tube and the core concrete and establish the shear strength formula of the core concrete; (3) To propose the composite shear stiffness formula incorporating the plastic development effect of the core concrete, and the overall process of the torsional moment vs. shear strain (T–γ) relation; (4) To propose the formula of torsional ultimate bearing capacity of circular CFT columns and compare its precision with those from the existing formulas.

2. Finite element modelling

2.1 Finite element models

Finite element (FE) models are established using the commercially available FE package ABAQUS version 6.10. In these models, the 8-node reduced integral format 3D solid element (C3D8R) is chosen to model the core concrete, steel tube and cover plate. The structured meshing technique is adopted as shown in Fig. 1.

In the FE models, a surface to surface contact was adopted for the interaction of steel tube and core concrete, of which the inner surface of steel tube was the master surface as well as the external surface of core concrete as the slave surface. Limited glide was adopted for Glide formula while the discretization method was surface to surface, and the "adjust only to remove overclosure" option was used in order to prevent any overclosure that could occur. Normal behavior and tangential behavior were used in contact property to simulate the bond-glide action between steel tube and core concrete.

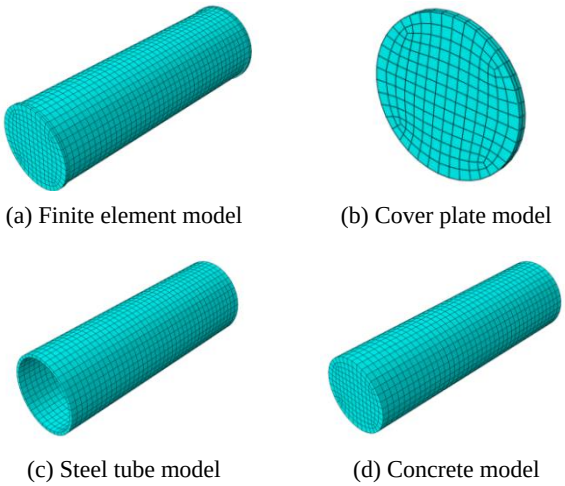

(a) Finite element model (b) Cover plate model

(c) Steel tube model (d) Concrete model

Fig. 1 Mesh generation of different models

The normal behavior was set as "hard" contact, allowing separation after contact, and the "penalty" function formulation were chosen for the tangential behavior. The friction coefficient between the steel tube and the core concrete was indicated from 0.3 to 0.6 by essential researches conducted by Baltay and Gjelsvik (1992). In this study, a friction coefficient of 0.5 was adopted thereby, which was identified by the prior research (Ding *et al*. 2011a) and fell in the above scope.

The sliding formulation is finite sliding in the contact interaction. The "tie" option is adopted for the constraint between the steel tube and the cover plate so that no relative motion occurs between them. To model the decrease portion of load-bearing capacity of specimens, torsional moment is applied using displacement control on the reference point coupling to the cover plate and both material and structural nonlinearities are considered and solved using the incremental-interactive method in ABAQUS.

Atriaxial concrete constitutive model in CFT columns has been presented by Ding *et al*. (2011a) through modifying the concrete model under tri-axial compression given by Ottosen and Ristinmaa (2005). The following stress-strain relationship is adopted in the model.

$$y=\begin{cases}\dfrac{A_n x+(B_n-1)x^2}{1+(A_n-2)x+B_n x^2} & x\le 1\\ \dfrac{x}{\alpha_n(x-1)^2+x} & x>1\end{cases} \tag{1}$$

where, A_n is the ratio of the initial tangent modulus to the secant modulus at peak stress, and the initial tangent modulus is equal to the elastic modulus. B_n is a parameter to control the decrease of elastic modulus at the ascending branch of the axial stress-strain relationship. α_n is for the descending branch of the axial stress-strain relationship.

In compressive zone, $y = \sigma/f_c$ and $x = \varepsilon/\varepsilon_c$ are the stress and strain ratios of the core concrete to the uniaxial compressive concrete respectively. σ and ε are the stress and strain of the core concrete. $f_c = 0.4f_{cu}^{7/6}$ is theuniaxial compressive strength of concrete, where f_{cu} is the compressive cubic strength of concrete. ε_c isthestrain corresponding with the peak compressive stress of concrete, where $\varepsilon_c = 383f_{cu}^{7/18}\times10^{-6}$. $A_1 = 9.1f_{cu}^{-4/9}$, $B_1 = 1.6(A_1 - 1)^2$. $\alpha_1 = 0.15$. In tensile zone, $y = \sigma/f_t$ and $x = \varepsilon/\varepsilon_t$ are the stress and strain ratios of the core concrete to the uniaxial tensile concrete respectively. $f_t = 0.24f_{cu}^{2/3-}$ is the uniaxial tensile strength of concrete. $\varepsilon_t = 33f_{cu}^{1/3}\times10^6$ is the strain at peak uniaxial tension. $A_2 = 1.306$, $B_2 = 5(A_2 - 1)^2/3 = 0.15$, $\alpha_2 = 0.8$. More information of the tri-axial concrete model can be referred in Ding *et al.* (2011a).

This damage plasticity concrete model is based on the fitting of the stress-strain relation of concrete under uniaxial stress, and combined with parameters of strength criterion of concrete under multi-axial stresses and other parameters defined below, which is verified to simulate the stress-strain relation of concrete under uniaxial, biaxial and triaxial stress. What's more, this concrete model was validated in modelling triaxial compressed concrete of circular CFT stub

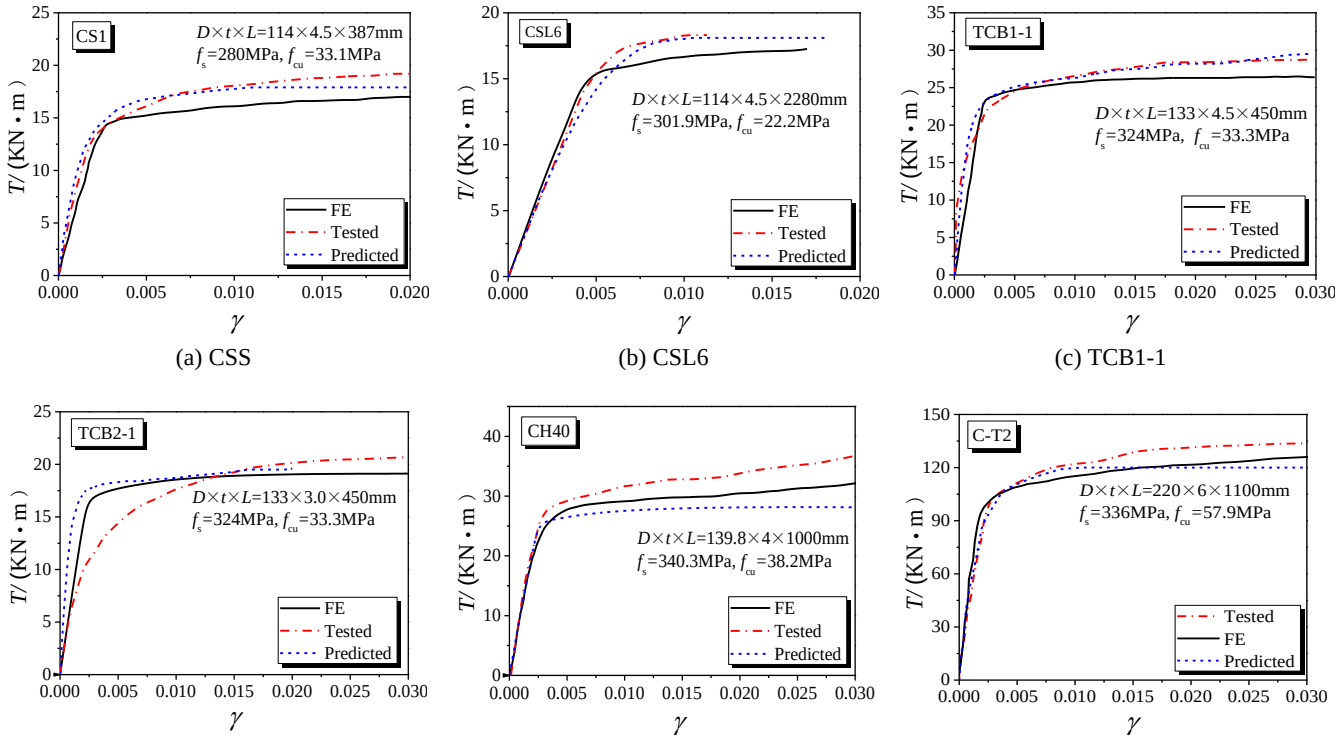

(a) CSS (b) CSL6 (c) TCB1-1

(d) TCB2-1 (e) CH-40 (f) C-T2

Fig. 2 Comparison of T–γ curves between FE results, tested results and predicted results

columns in our team (Ding *et al*. 2017).The parameters in ABAQUS were defined by Ding *et al*. (2011b): The eccentricity is 0.1; the ratio of initial equibiaxial compressive yield stress to initial uniaxial compressive yield stress (f_{b0}/f_{c0}) is 1.225; the ratio of the second stress invariant on the tensile meridian to that on the compressive meridian is 2/3; the viscosity parameter is taken as 0.005; and the dilation angle is 40°. Therefore, the damage plasticity model above is thereby adopted to investigate the mechanical behavior of circular CFT columns under pure torsion.

An elasto-plastic model, considering Von Mises yield criteria, Prandtl-Reuss flow rule, and isotropic strain hardening, was used to describe the constitutive behavior of steel. The expression for the stress-strain relationship of steel is as follows by Ding *et al*. (2011a)

$$\sigma_i = \begin{cases} E_s\varepsilon_i & \varepsilon_i \le \varepsilon_y \\ f_s & \varepsilon_y < \varepsilon_i \le \varepsilon_{st} \\ f_s + \zeta E_s(\varepsilon_i - \varepsilon_{st}) & \varepsilon_{st} < \varepsilon_i \le \varepsilon_u \\ f_u & \varepsilon_i > \varepsilon_u \end{cases} \quad (2)$$

where σ_i is the equivalent stress and f_u equals to $1.5f_s$, which corresponds to the yield strength. E_s is taken to be 2.06×10^5 MPa. ε_i is the equivalent strain, while ε_y is the strain when steel yields. ε_{st} is the strain when steel reinforcement equals to $12\varepsilon_y$. ε_u is the strain when the steel reaches ultimate strength and equals to$120\varepsilon_y$, and ζ equals to1/216.

The Prandtl-Reuss flow rule, which can be applicable to three-dimensional stress analysis, is used to the constitutive relationship of the steel tube, for the elastic part is considered into the increment in strain during the process of plastic deformation.

2.2 Validation of FE models

The comparison of torsional moment vs. shear strain (T–γ) curves between the tested results (Xu and Zhou 1991, Han *et al.* 2007, Beck and Kiyomiya 2003, Nie *et al.* 2012) and the corresponding FE modelling results are presented in Fig. 2, where D is the external diameter, t is wall thickness of the steel tube respectively and L is the length of CFT columns. It is seen that good agreement is achieved in both the elastic stage and the elastic-plastic stage. Except for the Fig. 2(d), which the stiffness of the curve obtained from the test results was slightly smaller than that of the FE modelling results. Compared with the test results of the

Table 1 Proposed formulas of torsional ultimate bearing capacity

Number	Formulas		Ref.
1	$T_u = v^t W_{sc}{}^t\tau_{sc}{}^y$ $T_{sc}{}^y = (0.422 + 0.313\alpha^{2.33})\xi^{0.134}f_{sc}{}^y$; $v^t = -0.3937\xi + 1.8157\xi^{0.5}$	(14)	Han *et al.* (2007)
2	$T_u = 1/(0.216e8.7\alpha$ $+ 0.235\alpha + 12.25)$ $+ \xi/(16.47\alpha^2 + 2.94\alpha + 4.9)f_cD^3$	(15)	Nie *et al.* (2012)
3	$T_u = W_T f_{sv}$ $W_T = \pi r_o{}^3/2$	(16)	GB 50936 (2014)
4	$T_u = 0.7A_sf_sR$	(17)	Xie and Zha (2012)

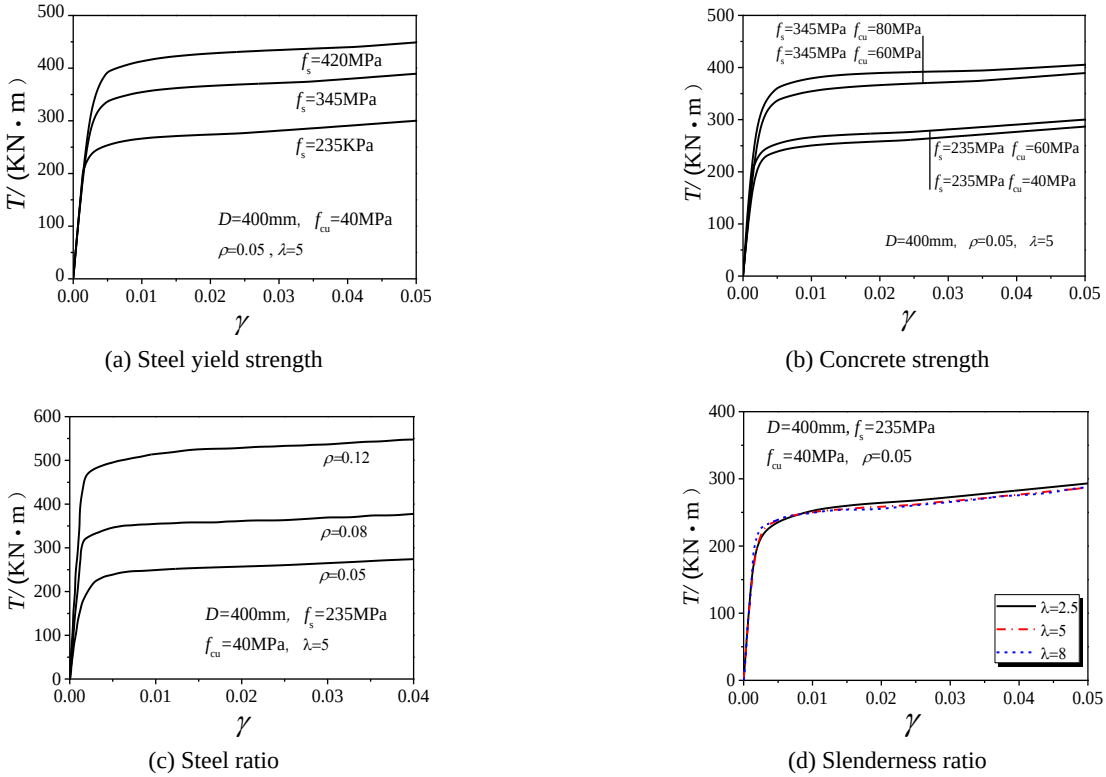

(a) Steel yield strength (b) Concrete strength

(c) Steel ratio (d) Slenderness ratio

Fig. 3 Parametric analysis on T-γ curves

Table 2 Comparisons between the tested results and the predicted results

Specimens	D (mm)	f_s (MPa)	f_{cu} (MPa)	t (mm)	$T_{u,c}$ (kN·m)	L (mm)	$T_{u,c}/T_{u,e}$						Ref.
							FE	Eq. (13)	Eq. (14)	Eq. (15)	Eq. (16)	Eq. (17)	
CSS6	114	301.9	21.9	4.5	19	800	1.092	1.015	0.965	1.251	1.084	1.019	Xu and Zhou (1991)
CSM6	114	301.9	20.6	4.5	18.5	1480	1.156	0.994	0.944	1.228	1.114	0.993	
CSL6	114	301.9	22.2	4.5	17.8	2280	1.085	0.950	0.902	1.170	1.158	0.955	
TCB1-1	133	324.3	33.3	4.5	28.9	450	1.064	1.099	1.020	1.174	1.049	1.054	Han *et al.* (2007)
TCB2-1	130	324.3	33.3	3	17.2	450	1.006	0.909	0.932	0.990	1.135	0.974	
TB1-1	133	324.3	30.4	4.5	28.1	2000	1.099	1.048	1.006	1.163	1.079	1.025	
TB2-1	133	324.3	30.4	3	16.8	2000	0.925	1.155	0.942	1.264	0.839	1.317	
CH35	139.8	322.9	36.3	3.5	27.1	1000	1.106	1.062	1.021	1.158	0.965	1.145	Beck and Kiyomiya (2003)
CH40	139.8	348.2	31.8	4	27.2	1000	1.063	0.997	0.878	0.940	1.324	0.835	
CH45	139.8	340.3	38.2	4.5	33.4	1000	1.132	0.900	1.119	1.228	0.940	1.176	
C-T1	220	285	54.4	4	86	1100	1.241	1.164	1.522	1.070	0.765	1.445	Nie *et al.* (2012)
C-T2	220	336	57.9	6	120	1100	1.091	1.010	1.181	1.031	0.961	1.150	
Average							1.095	1.012	1.039	0.093	1.032	1.092	
Coefficient dispersion							0.071	0.081	0.163	0.093	0.140	0.147	

same experimental group in Fig. 2(c), which has a good agreement between the two curves, the deviation of stiffness deviation in Fig. 2(d) might be caused by the experimental error, and it was also explained by Han *et al.* (2007). In the strain hardening stage, the curves keep going upwards for tested results and FE modelling results which shows good ductility for circular CFT columns under pure torsion. Table 2 gives the torsional ultimate bearing capacity comparisons between the tested results ($N_{u,1}$) and the FE results ($N_{u,0}$). The average value of $N_{u,1}/N_{u,0}$ is 1.095 and the coefficient dispersion is 0.071, which indicates the satisfactory correspondence between the tested and the FE results. With such validation, the FE models and the material constitutive models adopted in this study are confirmed to be reasonable and adequate.

2.3 Parametric study

To further understand the influence of different

parameters on the performance of circular CFT columns under pure torsion, a total of 45 FE full-scale models based on the validated FE modelling approach are developed. The parameters considered in the analysis include steel strength (f_s), concrete strength (f_{cu}), steel ratio (ρ, area ratio of steel tube to total cross section), and slenderness ratio. For all FE models, the steel tube diameter D is 400 mm and the specimen length L is 1000 mm.

(a) Steel strength

Fig. 3(a) presents the effect of the steel strength on the torsional T–γ curves. The steel strengths are Q235, Q345 and Q420, respectively with other parameters kept the same. It can be found that with the increase of the steel strength, the ultimate moment is improved by 47% and 17% respectively, while the composite shear stiffness almost remains the same in the elastic stage. The results indicate that the steel strength significantly influences the ultimate bearing capacity of the CFT columns.

(b) Concrete strength

Comparisons of the T–γ curves with various concrete strengths are given in Fig. 3(b). The concrete strength is C40, C60 paired with steel strength Q235, and C60, C80 paired with Q345 respectively. It is observed that with the increase of the concrete strength, the ultimate moment is slightly improved by less than 5%, and the composite shear stiffness almost remains unchanged. It can be concluded that the concrete strength has marginal effects on the mechanical performance of CFT columns.

(c) Steel ratio

The steel ratio is an important parameter for CFT columns which has been extensively investigated in the previous research work. Fig. 3(c) illustrates the effect of the steel ratio on the T–γ curves where the steel ratio is 0.05, 0.08 and 0.12 respectively. It can be found that with the increase of steel ratio, the composite shear stiffness is improved by 6.8% and 2.1% and the ultimate moment is improved by 43% and 45% respectively. Therefore, the increase of steel ratio helps increase obviously both the composite shear stiffness and the ultimate bearing capacity.

(d) Slenderness ratio

The slenderness ratio of circular CFT columns is defined as $\lambda = L/D$ in Chinese code GB 50936 (2014), where L is the calculated length of the column and D is the outer diameter of the steel tube. When $L/D < 4$, the circular CFT columns were often regarded as a stub column, and when $L/D > 4$, the columns were non-stub columns. Comparisons of the T–γ curves with different slenderness ratio are shown in Fig. 3(d). It is found that the slenderness ratio almost have no significant influence on the T–γ curves with slenderness ratios ranging from 2.5 to 8.Therefore, it can be confirmed that the torsional behavior of circular CFT columns are the same regardless of the slenderness ratio.

2.4 The confinement effect analysis

To give a comprehensive understanding of the confinement effect between the steel tube and the core concrete which greatly enhanced the mechanical performance of circular CFT columns under pure torsion, the confinement effect between the steel tube and the core concrete is analyzed below. The calculating conditions of circular CFT specimens are: D = 400 mm, L = 1000 mm, ρ = 0.05, f_s = 235 MPa, f_{cu} = 40 MPa.

2.4.1 The core concrete

Fig. 4 displays the comparison of maximal shear stress (τ) vs. shear strain (γ) curves between the core concrete (τ_{cc}) and the corresponding unconfined plain concrete (τ_c) under pure torsion. It is seen that the torsional behaviors are the same in the elastic stage for both core concrete and plain concrete. However, in the elastic-plastic stage and failure stage, large deviation is observed between the two curves. For plain concrete the brittle failure occur when the maximal shear stress reaches its shear strength, and then, the shear stress declines rapidly with the increase of the shear strain, as demonstrated in mechanics of materials theory. For core concrete in CFT columns, due to the confinement effect between the steel tube and the core concrete, the maximal shear strength and ductility of core concrete grow much higher than those of the counterpart unconfined plain concrete.

Fig. 5 presents the interaction stress σ_{cp} (σ_{cp} equals CPRESS stress in ABAQUS divided by the Coulomb friction coefficient) and strain relation of the core concrete in CFT column under pure torsion and axial compression, respectively. The interaction stress σ_{cp} can reflect the contact stress in the normal direction between the core concrete and the steel tube. It can be seen from Fig. 5(a) that in the early stage (before the two σ_{cp}-γ curves separate at 500 $\mu\varepsilon$ point, also seen in Fig. 4), the value of σ_{cp} is close to 0, which indicates that almost no confinement effect generates between the core concrete and the steel tube, therefore the torsional behavior of the core concrete and the corresponding plain concrete in the elastic stage behaves the same. In the later stage, the σ_{cp} increases linearly as well as the τ_{cc} of the core concrete. In the end, the σ_{cp} keeps stable after 6000 $\mu\varepsilon$ reached, therefore the τ_{cc} of the core concrete keep stable as well as the confinement effect. Finally, from all the analysis above, the conclusion that the confinement effect between the steel tube and the core concrete is the main reason that greatly improves the shear strength and ductility of the core concrete, therefore, can be proposed.

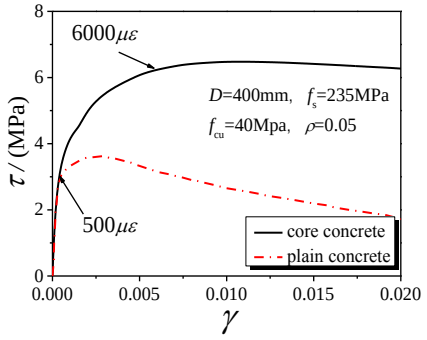

Fig. 4 Comparison of τ–γ curves between the core concrete and the plain concrete

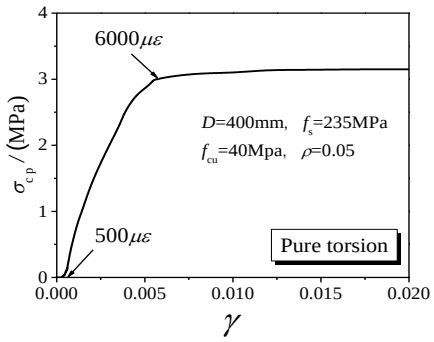

(a) Pure torsion

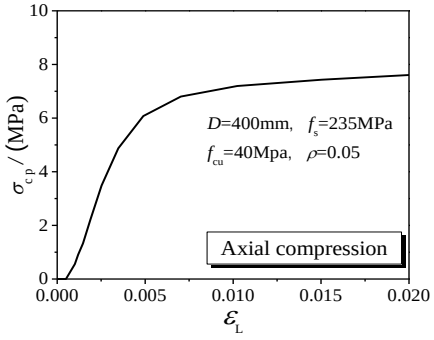

(b) Axial compression

Fig. 5 The interaction stress-strain relation of concrete

Fig. 5(b) shows the relation of σ_{cp} and axial strain (ε_L) of the same core concrete in circular CFT column subjected to axial compression. It can be found that the development process of σ_{cp} is similar to that under pure torsion and the value of σ_{cp} is about 2.7 times in the ultimate stage than the corresponding σ_{cp} under pure torsion.

Fig. 6 compares the shear stress contours of core and plain concretes at the failure stage. It is seen that the distribution forms of shear stresses are similar, that is to say, the shear stress increases hierarchically inside-out, which is verified in Fig. 15. Therefore, the shear stress state of the core concrete in CFT column is greatly enhanced by the confinement effect from the steel tube.

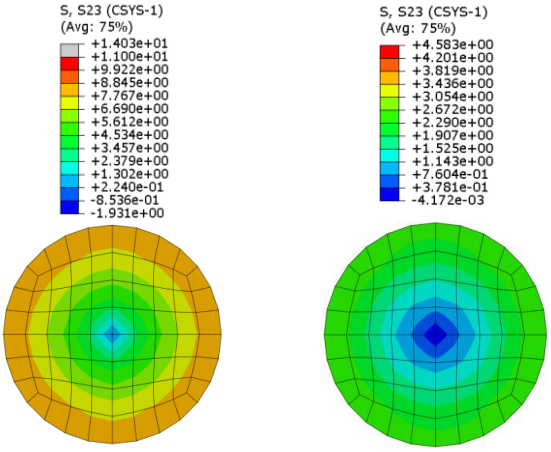

(a) Core concrete (b) Plain concrete

Fig. 6 Shear stress contours of core concrete and plain concrete

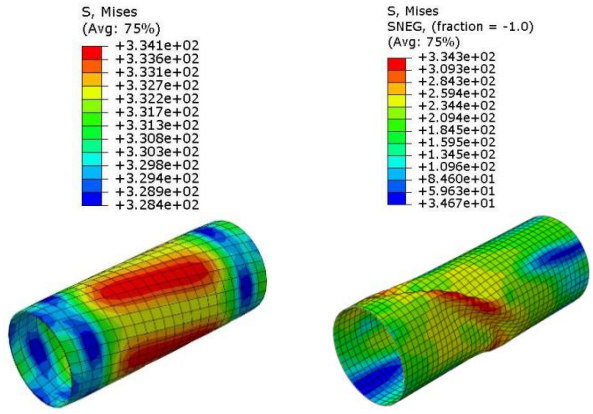

(a) Steel tube in CFT (b) HST

Fig. 7 Typical failure modes of steel tube in CFT column and HST

2.4.2 The steel tube

Fig. 7 shows the typical failure modes of steel tube in circular CFT column and the corresponding hollow steel tube (HST) under pure torsion. It is observed that significant difference is there between the typical failure modes for the two specimens. For HST, inclined outward buckling along 45° direction occurs, while the steel tube in CFT column exhibits good plastic and steady behavior because the local buckling is prevented by the inner core concrete under pure torsion. Consequently, the changes in buckling mode of the steel tube significantly improve the plastic deformation capacity of the circular CFT columns under pure torsion.

Fig. 8(a) presents the comparisons of typical T–γ curves between the steel tube in circular CFT column and that in the corresponding HST under pure torsion. It is found that in the elastic stage the torsional behaviors for the steel tubes from both columns are the same. In the elastic-plastic stage, the ultimate moment of the steel tube in CFT column is slightly higher than that in HST. This is due to the uniaxial tension is produced in the steel tube because of the expansion of the core concrete under pure torsion. It makes the stress state of the steel tube in CFT column become biaxial stress state rather than uniaxial stress state in the corresponding HST (Xu and Zhou 1991). Besides, no descending branch appears in the T–γ curve of the steel tube in CFT column, which is attributed to the improved stability and ductility with prevention of local bulking. Fig. 8(b) compares 45 FE modelling results on the ultimate bearing capacity of the steel tube in CFT column (T_s) with that from the corresponding HST (T_s^P). It can be seen that the ultimate bearing capacity of steel tube in CFT columns is improved by less than 6% compared with that in the corresponding HST. Though the confinement effect between the steel tube and the core concrete improves the plastic deformation capacity of the steel tube, the ultimate bearing capacity is not significantly improved, and thereby, it can be estimated by that of the steel tube from the corresponding HST columns.

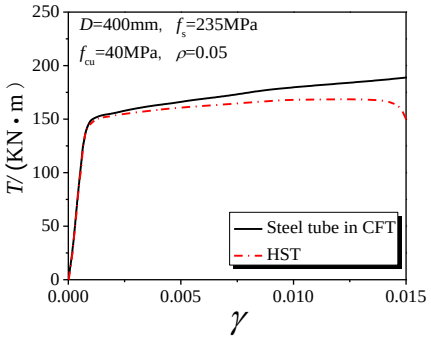

(a) Typical T–γ curves

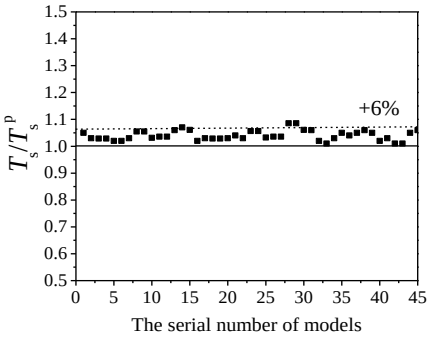

(b) Various T_s/T_s^P

Fig. 8 Comparisons between the steel tube in CFT column and the corresponding HST

3. Design approach

3.1 Shear stress of the core concrete

The above analysis has indicated the improvement of maximal shear stress of the core concrete (τ_{cc}) compared with the corresponding shear stress of the plain concrete (τ_c) due to the confinement effect between the core concrete and the steel tube. In order to establish the formula to calculate the shear strength of the core concrete and to propose the ultimate bearing capacity of the core concrete under pure torsion, parametric study based on the validated FE modelling approach are conducted to investigate the effect of various parameters on the ratio of τ_{cc}/τ_c. The parameters considered in the analysis include steel strength (f_s), concrete strength (f_{cu}), steel ratio (ρ) and external diameter (D).

The τ_{cc}/τ_c–ρ curves with different parameters are presented in Fig. 9. It can be seen that with the increase of the steel ratio from 0.05 to 0.12, the ratio of τ_{cc}/τ_c increases almost proportionally from 1.7-2.8. Further than that, the influence of the steel strength, concrete strength and external diameter are very limited on the ratio of τ_{cc}/τ_c. Therefore, it is concluded that the steel ratio is the main factor that affects the ratio of τ_{cc}/τ_c.

Fig. 10 presents the FE results of τ_{cc}/τ_c–ρ relationsof the core concrete in circular CFT columnsand the regression relation of τ_{cc}/τ_c–ρ can use the following Eq. (3). Comparisons shows the average value of the FE results divided by the predicted results using Eq. (3) is 1.024 and the coefficient dispersion is 0.062, where reasonable agreement is achieved.

$$\tau_{cc} = (1 + 16.24\rho)\tau \tag{3}$$

For counterpart unconfined plain concrete, the relation of the maximal shear stress (τ_c) and the corresponding axial compressive strength (f_{cu}) can be expressed as

$$\tau_c = 0.37 f_{cu}^{0.62} \tag{4}$$

Fig. 11 compares the τ_c–f_{cu} relation of tested results conducted by Shi (1999) with predicted results by Eq. (4). The average value of the tested results divided by the predicted results is 0.935 and the coefficient dispersion is 0.070. Therefore, the shear strength of the core concrete in circular CFT columns can be estimated by Eq. (3) and Eq.

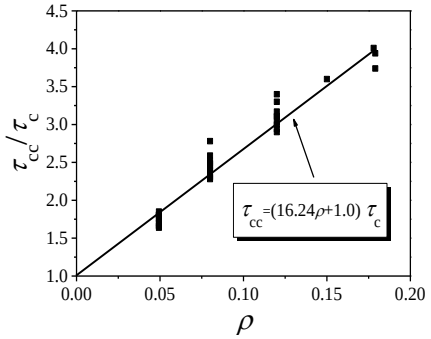

Fig. 10 Regression results of τ_{cc}/τ_c~ρ relation

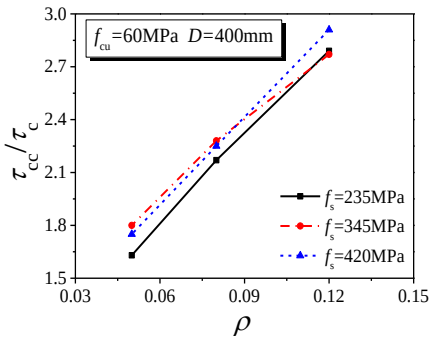

(a) Steel yield strength

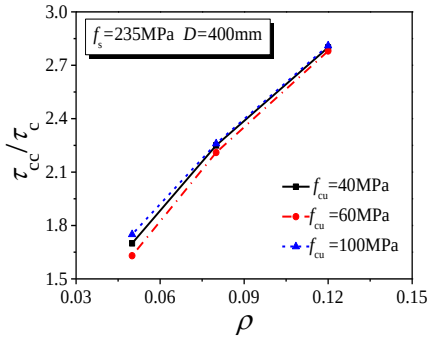

(b) Concrete strength

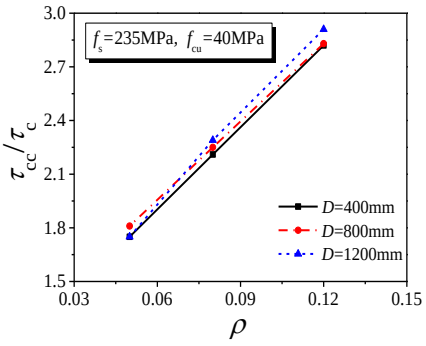

(c) External diameter

Fig. 9 Parameters studies of τ_{cc}/τ_c–ρ relation

(4) as follows.

$$\tau_{cc} = (0.37 + 6\rho) f_{cu}^{0.62} \quad (5)$$

3.2 Ultimate shear strain

From the typical T–γ curves of circular CFT columns under pure torsion, it is observed that after the ultimate bearing capacity reached, the torsional moment tends to be stabilized and no descending branch appears. Therefore, the ultimate shear strain ($\gamma_{sc,u}$) of circular CFT columns under pure torsion need to be defined. Fig. 12 gives the ultimate shear strain of 45 FE modelling results when the ultimate moment reached. It can be seen that all ultimate shear strain results range from 0.0075 to 0.012. For practical consideration and the practical stress of the steel tube, 0.01 is set as the ultimate shear strain of the circular CFT columns, and the corresponding torsional moment is the ultimate bearing capacity of the circular CFT columns in this paper. This definition is also given by Han *et al.* (2007).

3.3 Composite shear stiffness

The composite shear stiffness of composite members is typically computed in GB 50936 (2014) and CECS28 (2012) using the following equation.

$$G_{sc}A_{sc} = G_sA_s + G_cA_c \quad (6)$$

where, $G_{sc}A_{sc}$ is thecompositeshear stiffness, G_{sc} is the composite shear modulus. G_s and G_c are the shear modulus of the steel and the concrete, A_{sc} is the section area, A_s and A_c are the area of the steel tube and the concrete. It can be seen in Eq. (6) that the composite shear stiffness of CFT column is linearly added together by the shear stiffness of the steel tube and the concrete, where the shear modulus reduction of the core concrete caused by the plastic development is not concerned.

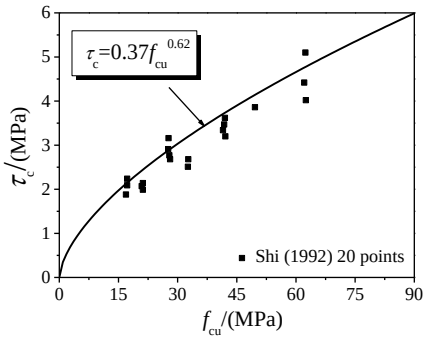

Fig. 11 Comparison of predicted and tested values

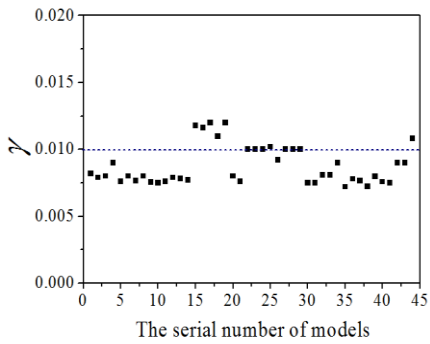

Fig. 12 FE results of the ultimate shear strain ($\gamma_{sc,u}$)

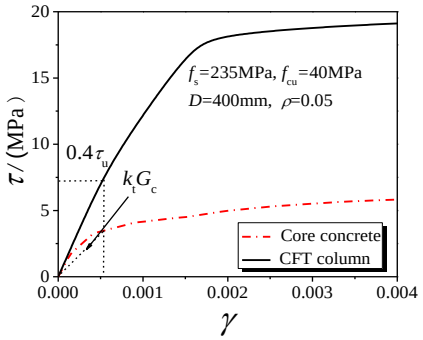

(a) ρ = 0.05

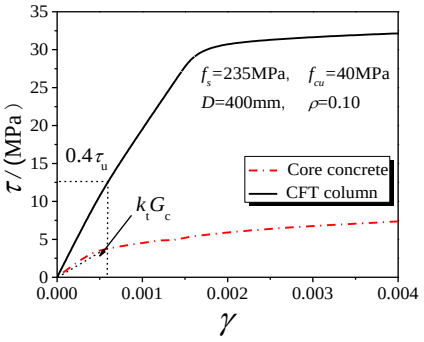

(b) ρ = 0.10

Fig. 13 Comparisons of the τ–γ curve for CFT column and the corresponding core concrete in two steel ratio

According to FE modelling results and Ding *et al.* (2011b), the composite shear stiffness of CFT columns is defined as the secant stiffness corresponding to a shear stress of 0.4τ_u in the τ–γ curve in general ($\tau = T/W_{sc}$, W_{sc} is the torsional section factor, $W_{sc} = \pi D^3/16$ and τ_u is the ultimate maximal shear stress). It should be mentioned that the circular CFT column is considered as a unified member here. The composite shear stiffness can be expressed as

$$G_{sc}A_{sc} = G_sA_s + k_tG_cA_c \quad (7)$$

where: k_t is defined as the plastic development factor of the core concrete. The comparisons of the τ–γ curves between the circular CFT columns and the corresponding core concrete in steel ratio of 0.05 and 0.10 are presented in Fig. 13, respectively. It is found that when 0.4τ_u is reached, the unified CFT column is still in the elastic stage while the inner core concrete is in the elastic-plastic stage and the secant modulus of the core concrete is reduced to be k_tG_c. Besides, with the increase of the steel ratio from 0.05 to 0.10 (seen in Fig. 13(b)), the process of plastic development of the core concrete is reduced thus the k_t is closer to 1.0 which means less plastic development generates for the core concrete.

Fig. 14 gives the calculated k_t–ρ relation results of 45 FE models. It is seen that with the increase of the steel ratio, k_t

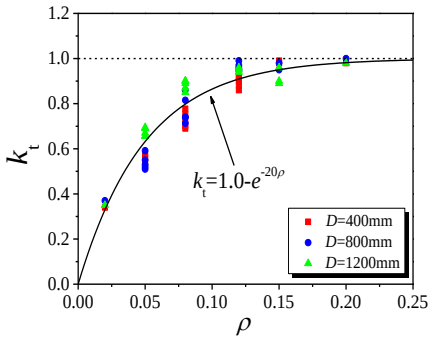

Fig. 14 FE results of k_t–ρ relation and regression curve

is approaching to 1 nonlinearly and the influence of external diameter, steel strength and concrete strength on k_t value in the same steel ratio is limited in 15%. For practicability and convenience, the steel ratio can be considered as the main factor that affects k_t evaluation. Therefore, based on the FE results and regression analysis, k_t is expressed in Eq. (8). The comparison between the FE results and the calculated results of k_t shows the average value is 1.016 and the coefficient dispersion is 0.132 where satisfactory correspondence is achieved.

$$k_t = 1 - e^{-20\rho} \tag{8}$$

3.4 Ultimate bearing capacity

3.4.1 Formulas

From the above analysis, the ultimate bearing capacity of circular CFT columns under pure torsion can be assembled by the ultimate bearing capacity of steel tube and core concrete together. The formula of ultimate bearing capacity of the steel tube can be replaced by that of the corresponding HST which is verified before, and for the core concrete, the formula given in mechanics of materials theory considering the shear strength of the core concrete proposed above can be adopted. Therefore, the formula of ultimate bearing capacity of circular CFT columns can be expressed as

$$T_u = T_s + T_c \tag{9}$$

where: T_u is the ultimate bearing capacity of circular CFT columns, T_s and T_c are the ultimate bearing capacity of the steel tube and the core concrete respectively.

For the steel tube, the shear stress is assumed constant along the wall thickness direction. Thin-wall tube theory defines the relationship between the shear stress and the torsional moment as follows

$$T_s = 2A_{so}t\tau_s \tag{10}$$

where: A_{so} is the areas made by the average thickness of the steel tube, τ_s is the average shear stress of the steel tube at ultimate state.

The relation between τ_s and f_s can be expressed as below in material strength theory.

$$\tau_s = f_s/\sqrt{3} \tag{11}$$

For the core concrete, the typical τ_{cc}–γ curve and the shear stress distribution along thickness direction under pure torsion are presented in Fig. 15 respectively. It is found that the distribution of the shear stress is approximately proportional. Therefore the shear stress of the core concrete is supposed linear distribution on the safe side. The ultimate bearing capacity of the core concrete incorporating Eq. (5) can be expressed as follow

$$T_c = \frac{2}{3}\pi r^3 \tau_{cc} \tag{12}$$

where: r is the radius of the core concrete.

From Eqs. (9)-(12), the formula of ultimate bearing capacity of circular CFT columns under pure torsion is simplified as

$$T_u = 1.15A_{so}tf_s + 0.67A_c r\tau_{cc} \tag{13}$$

where: τ_{cc} is the shear strength of the core concrete. $\tau_{cc} = (0.37 + 6.0\rho)f_{cu}^{0.62}$.

3.4.2 Proportion of the ultimate torsional moment

To further understand the ultimate torsional moment distribution between the steel tube and the core concrete, the T_s/T_u~ρ andT_c/T_u~ρ relations of circular CFT columns under pure torsion are given in Fig. 16 respectively. It is seen that the ultimate moment beard by the steel tube (T_s/T_u) increases almost linearly from 0.6-0.7 with the increase of the steel ratio and that beard by the core concrete (T_c/T_u) declines linearly from 0.4-0.3 reversely. Besides, the influence of different external diameter, steel strength and concrete strength on the ratio in the same steel ratio is within 15%.

3.4.3 Formulas validation

The predicted results using the Eq. (13) ($N_{u,1}$) are compared with the FE results ($T_{u,0}$) as shown in Fig. 17. The average value of $N_{u,1}/N_{u,0}$ is 1.074 and the coefficient dispersion is 0.043, which confirmed the precision of the proposed Eq. (13).

Formulas of ultimate bearing capacity proposed by other investigators and codes are listed in Table 1. It can be seen that those formulas vary significantly in form and practicability. Table 2 displays the comparisons between the tested results ($T_{u,c}$) and the predicted results using FE modelling ($T_{u,0}$), Eq. (13) ($T_{u,1}$), and Eqs. (14)-(17). The

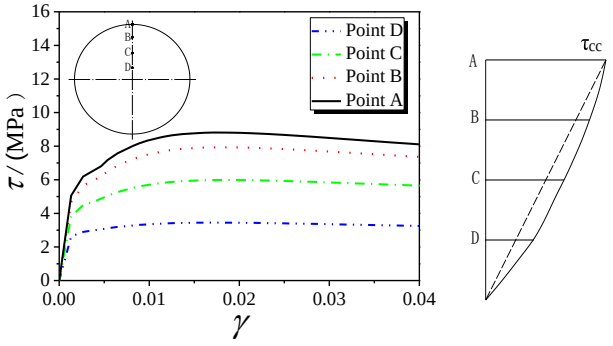

Fig. 15 Shear stress distribution of the core concrete

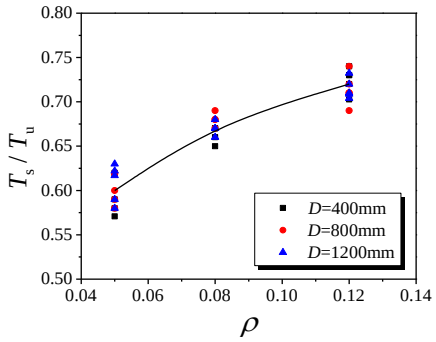

(a) T_s/T_u~ρ results

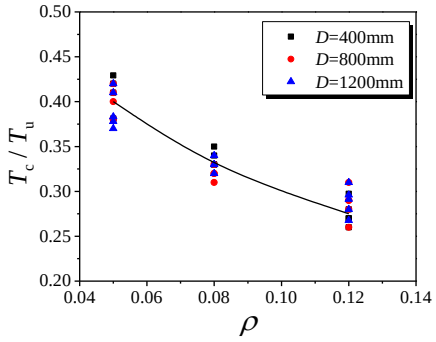

(b) T_c/T_u~ρ results

Fig. 16 Proportion of ultimate torsional moment shared by steel tube and concrete

results show that the average value of $T_{u,c}/T_{u,1}$ is 1.012 and the coefficient dispersion is 0.081. Therefore, good agreement is achieved between the predicted results using Eq. (13) and the tested results and the predicted results are at the safe side. Furthermore, the results from Eq. (13) have the best precision compared with other formulas listed in Table 1.

3.5 Torsional moment versus shear strain relation

Based on the proposed formulas of ultimate bearing capacity (T_u) and composite shear stiffness in this paper, a simplified model to predict the overall process of the torsional moment (T) vs. shear strain (γ) relation of the circular CFT columns under pure torsion is developed. The T–γ relation is expressed as

$$y = \begin{cases} \dfrac{kx + (m-1)x^2}{1 + (k-2)x + mx^2} & x' \le 1 \\ 1 & x' > 1 \end{cases} \tag{14}$$

where: $y = T/T_u$, $x = \gamma/\gamma_{sc,u}$; $k = G_{sc}W_{sc} \times \gamma_{sc,u}/T_u$; $m = 1.67(k - 1)^2$. A horizontal straight line is assumed for T–γ curves after the ultimate bearing capacity is reached for convenience. Fig. 2 shows comparisons of the T–γ curves between the tested results, FE results and the predicted results using Eq. (18). It can be seen that good agreement is obtained in general. Therefore, the Eq. (18) is able to describe the torsional behavior of the entire loading history of CFT columns under pure torsion.

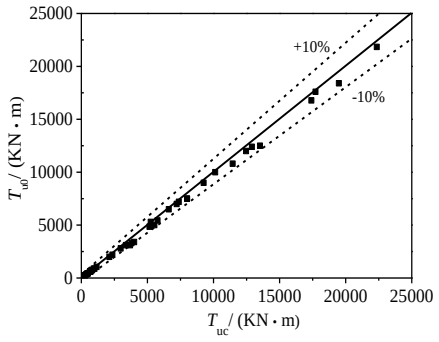

Fig. 17 Comparisons of FE results and predicted results

4. Conclusions

This paper presents a combined numerical and theoretical study on the behavior of circular CFT columns under pure torsion. Based on the validated FE model, parametric study is conducted to understand the influence of different parameters on the mechanical performance of circular CFT columns. The confinement effect between the core concrete and the steel tube are analyzed in detail and formulas to calculate the ultimate bearing capacity and composite stiffness of circular CFT columns under pure torsion are proposed. Finally, the conclusions can be drawn as the follows:

- Finite element models based on reasonable concrete constitutive model are established and validated by experimental results. Parametric study indicates that the steel strength and steel ratio influence distinctly the torsional behavior of circular CFT columns while the concrete strength and slenderness ratio influence slightly.
- The analytical results indicates that the confinement effect between the core concrete and the steel tube greatly improves the plastic deformation capacity of the steel tube and enhances the shear strength of the core concrete under pure torsion and thereby the shear strength formula of the core concrete is established.
- The shear stiffness of circular CFT columns is reduced due to the plastic development of the core concrete under pure torsion, therefore, the composite shear stiffness formula of circular CFT columns considering the torsional plastic development factor k_t is proposed. Besides, a practical approach is proposed to express the overall process of the torsional moment vs. shear strain relation.
- The formula of torsional ultimate bearing capacity of circular CFT columns is proposed and the precision and practicability of proposed formula is verified to be well satisfied compared with tested results and existing formulas.

Acknowledgments

This research work was financially supported by the

National Key Research Program of China, Grant No. 2017YFC0703404.

References

Baltay, P. and Gjelsvik, A. (1992), "Coefficient of friction for steel on concrete at high normal stress", *J. Mater. Civil Eng.*, **2**(1), 46-49.

Beck, J. and Kiyomiya, O. (2003), "Fundemental pure bearing properties of concrete filled steel tubes", *Proceedings of the Japan Society of Civil Engineers*, **739**(739), 285-296.

CECS28 (2012), Technical specification for concrete-filled steel tubular structures, China planning press; Beijing, China.

Chang, X., Ru, Z. and Zhou, W. (2013), "Study on concrete-filled stainless steel carbon steel tubular (CFSCT) stub columns under compression", *Thin-Wall. Struct.*, **63**(3), 125-133.

Ding, F.X., Ying, X.Y. and Zhou, L.C. (2011a), "Unified calculation method and its application in determining the uniaxial mechanical properties of concrete", *Front. Archit. Civ. Eng. China*, **5**(3), 381-393.

Ding, F.X., Yu, Z.W. and Bai, Y. (2011b), "Elasto-plastic analysis of circular concrete-filled steel tube stub columns", *J. Struct. Eng.*, **67**(10), 1567-1577.

Ding, F.X., Tan, L. and Liu, X.M. (2017), "Behavior of circular thin-walled steel tube confined concrete stun columns", *Steel Compos. Struct., Int. J.*, **23**(2), 229-238.

GB 50936 (2014), Technical code for concrete filled steel tubular structure, China building industry press; Beijing, China.

Han, L.H. Yao, G.H. and Tao, Z. (2007), "Performance of concrete-filled thin-walled steel tubes under pure torsion", *Thin-Wall. Struct.*, **45**(1), 24-36.

Ju, C., Wei, L.J. and Jun, F. (2008), "Experimental investigation of thin-walled centrifugal concrete-filled steel tubes under torsion", *Thin-Wall. Struct.*, **46**(10), 1087-1093.

Kim, D., Jeon, C. and Shim, C. (2016), "Cyclic and static behaviors of CFT modular bridge pier with enhanced bracings", *Steel Compos. Struct., Int. J.*, **20**(6), 173-191.

Kim, H.J., Ham, J. and Park, K. (2017), "Numerical study of internally reinforced circular CFT column-to-foundation connection according to design variables", *Steel Compos. Struct., Int. J.*, **23**(4), 235-247.

Kwak, J.H., Kwak, H.G. and Kim, J.K. (2013), "Behavior of circular CFT columns subject to axial force and bending moment", *Steel Compos. Struct., Int. J.*, **14**(2), 173-190.

Lee, E.T., Yun, B.H., Shim, H.J., Chang, K.H. and Lee, G.C. (2009), "Torsional behavior of concrete-filled steel tube columns", *J. Struct. Eng.*, **135**(10), 1250-1258.

Lee, S.H., Uy, B., Choi, Y.H. and Choi, S.M. (2011), "Behavior of high-strength concrete-filled steel tubular (CFST) column under eccentric loading", *J. Constr. Steel Res.*, **67**(1), 1-13.

Nie, J.G., Wang, Y.H. and Fan, J.S. (2012), "Experimental study on seismic behavior of concrete filled steel tube columns under pure torsion and compression–torsion cyclic load", *J. Constr. Steel Res.*, **79**(1), 115-126.

Ottosen, N.S. and Ristinmaa, M. (2005), "12-common plasticity models", In: *The Mechanics of Constitutive Modeling*, pp. 279-319.

Shi, S.S. (1999), "The shear strength, shear modulus and elastic modulus of concrete", *J. Civil Eng.*, **32**(2), 47-52. [In Chinese]

Wang, Q.T. and Chang, X. (2013), "Analysis of concrete-filled steel tubular columns with "T" shaped cross section (CFTTS)", *Steel Compos. Struct., Int. J.*, **15**(1), 41-55.

Xie, X.Y. and Zha, X.X. (2012), "Torsion and shear behavior study of hollow and solid concrete filled steel tubular members II: Theoretical research on strength", *Progress in Steel Building Structures*, **14**(3), 7-11.

Xu, J.S. and Zhou, J. (1991), "The experimental research of concrete filled steel tubular slender column under combined compression and torsion", *J. Harbin Inst. Constr. Eng.*, **24**, 43-50. [In Chinese]

CC